Research Article

Fault Diagnosis of Rolling Element Bearing Using an Adaptive Multiscale Enhanced Combination Gradient Morphological Filter

Yuanqing Luo [ID],[1] **Changzheng Chen** [ID],[1,2] **Shuang Kang**,[1] **and Pinyang Zhang**[1]

[1]*School of Mechanical Engineering, Shenyang University of Technology, Shenyang 110870, China*
[2]*Liaoning Engineering Center for Vibration and Noise Control, Shenyang 110870, China*

Correspondence should be addressed to Changzheng Chen; chencz6699@sina.com

The extraction of the vibration impulse signal plays a crucial role in the fault diagnosis of rolling element bearing. However, the detection of weak fault signals generally suffers the strong background noise. To solve this problem, a new adaptive multiscale enhanced combination gradient morphological filter (MECGMF) is proposed for the fault diagnosis of rolling element bearing. In this method, according to the filtering ability of four basic morphological filter operators, an enhanced combination gradient morphological operation (ECGMF) is first proposed. This design enhances the ability of MECGMF to extract impulse signals from strong background noise. And accordingly, a new adaptive selection strategy named kurtosis fault feature ratio (KFFR) is proposed to select an optimal structuring element (SE) scale. Subsequently, the optimal SE scale is the largest measure of multiscale morphological filtering for extracting bearing fault information. In the meanwhile, the effectiveness of the proposed method is verified by simulation and experiment. Finally, the experimental results demonstrate that MECGMF can effectively restrain the noise interference and extract fault characteristic signals of rolling element bearing from strong background noise. Moreover, comparative tests show that the proposed method is more effective in detecting wind turbine bearing failures.

1. Introduction

Rolling bearings are widely used as important components of mechanical equipment, such as aerospace, automotive, wind power, and some large mechanical equipment [1]. Their running state is directly related to the healthy running state of the mechanical system. Therefore, it is especially important for early fault identification of bearings. When the bearing fails locally, nonlinear and nonstationary shock signals are usually generated [2]. However, these fault signals are usually submerged in strong background noise. Therefore, how to effectively extract fault information from strong background noise becomes crucial.

In recent years, short-time Fourier transform (STFT) [3], stochastic resonance (SR) [4], wavelet transform (WT) [5], and empirical mode decomposition (EMD) [6] have been widely used to deal with nonlinear and nonstationary signals of faulty bearing. However, these methods usually have their own limitations. For instance, the time and frequency

resolution of the window function of STFT cannot be optimal at the same time. The system parameters of SR are not easy to be determined. WT filtering requires manual selection of wavelet bases, which is difficult to perform adaptively. EMD is affected by boundary effects and mode mixing.

Different from the aforementioned time-frequency processing method, the morphological filtering (MF) algorithm is a filtering method based on mathematical morphology [7]. Initially, Matheron and Serra applied morphological filtering for image processing [8]. At present, it is widely used in mechanical vibration signal processing [9]. By modifying the geometry of the time-domain signal, it can preserve the fault characteristics of the signal, and it can also effectively remove the noise signal. It is an effective nonlinear signal filtering processing method [10]. The morphological filtering theory mainly includes the selection of SE and morphological operators. For SE, it consists mainly of three parts: length, height, and shape. Some

scholars have already researched [11, 12] the height and shape of SE have less effect on the filtering results. Therefore, this paper will further study the performance of morphological filtering from the two aspects of the length of SE and the morphology operator.

In the signal processing process, morphological filtering mainly includes four basic operators: erosion, dilation, opening, and closing operators [7]. Erosion operator can reduce the signal peak and widen the signal valley. Closing operator can suppress the signal negative impulse. In contrast, dilation and opening operators are able to extract negative peak suppression positive peaks. Based on the aforementioned four basic operators, some advanced cascading and combining operations can be implemented. For example, Hu et al. [13] applied the morphological gradient (MG) operator to bearing fault diagnosis successfully. Also, Li et al. [14] used MG to propose weight multiscale morphological filtering. Raj and Murali [15] used the MG operator to extract the bearing fault characteristics. Osman and Wang [16] proposed a new morphological Hilbert–Huang (MH) technique to detect fault characteristics of bearings. Then, Wang et al. [17] used the combination morphological filter operator (CMF) to eliminate the high-frequency noise. However, these morphological operators only used the opening and closing characteristics which generally led to the different output bias. Aijun et al. [18] proposed a combined Top-Hat (CTH) morphological filter operator to extract the impulse signal of the bearing. Li et al. [19] enumerated and analyzed the characteristics of various morphological filter operators and proposed a new enhanced operation (MGPO). Based on the aforementioned research studies, in order to further enhance the ability of morphological operators, this paper proposed a new morphological operator named enhanced combination gradient morphological filter (ECGMF).

Therefore, the optimal scale selection of SE is critical to the performance of the filtering performance. The shorter its length, the more obvious the fault feature information extraction effect, but the noise suppression effect is not good. On the contrary, the longer its length, the more obvious the noise suppression effect but affects the extraction of fault characteristic information [20]. At present, there are a large number of scholars who study the adaptive selection method of structural element length. Some scholars use 0.6 times the length of SE as the empirically optimal length, but this is not accurate enough. Deng et al. [21] used envelope spectrum sparsity (IESS) to select the optimal scale of SE. Although his method can effectively extract the impulse characteristic signal, he ignores the details of the signal. Wu et al. [22] selected the optimal scale of SE based on the kurtosis criterion. Kurtosis has been proven to be effective at extracting the impulsive feature, but it is also vulnerable to be interfered [23]. Miao et al. [24] proposed a new fault detection standard named KR, which is proved as a comprehensive index for detecting bearing fault characteristics. This paper selects the product of the kurtosis value of the frequency domain and R_f as a measure. Therefore, a new vector factor (KFFR) is applied to select the optimal scale of MECGMF.

The rest of this paper is organized as follows: The new morphological filter method (i.e., MECGMF) with KFFR is proposed in Section 2. The specific scheme of the proposed method for bearing fault diagnosis is shown in Section 3. In Section 4, the proposed method is validated on the simulation signals. Section 5 presents experimental verification of the proposed method. Finally, the conclusions are drawn in Section 6.

2. Basic Theory of Mathematical Morphology

2.1. Morphological Filter.
Supposing the original input signal $f(n)$ is a discrete function defined in $F = (0, 1, \ldots, N - 1)$ and the SE $g(m)$ is also the discrete function defined in $G = (0, 1, \ldots, M - 1)$ $(N \geq M)$, respectively, the four basic operators (i.e., dilation, erosion, opening, and closing operators) can be defined as follows:

Dilation:

$$(f \oplus g)(n) = \max[f(n - m) + g(m)]. \tag{1}$$

Erosion:

$$(f \ominus g)(n) = \min[f(n + m) - g(m)]. \tag{2}$$

Opening:

$$(f \circ g)(n) = (f \ominus g \oplus g)(n). \tag{3}$$

Closing:

$$(f \cdot g)(n) = (f \oplus g \ominus g)(n), \tag{4}$$

where $\oplus$ denotes the dilation operator, $\ominus$ denotes the erosion operator, $\circ$ stands for the opening operator, and $\cdot$ stands for the closing operator. Besides, several main morphological filters [13] are introduced as follows:

Morphological gradient (MG):

$$MG(f(n)) = (f \oplus g)(n) - (f \ominus g)(n), \tag{5}$$

Difference filter (DIF):

$$DIF(f(n)) = (f \cdot g)(n) - (f \circ g)(n). \tag{6}$$

The opening-closing F_{OC} and closing-opening F_{CO} filters are defined as follows:

$$F_{OC}(f(n)) = (f \circ g \cdot g)(n),$$
$$F_{CO}(f(n)) = (f \cdot g \circ g)(n). \tag{7}$$

A combination morphological filter with F_{OC} and F_{CO} (CMF) is defined as

$$y(n) = \frac{F_{CO}(f(n)) + F_{OC}(f(n))}{2}. \tag{8}$$

F_{CO} and F_{OC} gradient operation ($G_{CO\&OC}$) [23]:

$$F_{CO\&OC}(f(n)) = (f \cdot g \circ g)(n) - (f \circ g \cdot g)(n). \tag{9}$$

Average combination difference morphological filters (ACDIF) [20]:

$$\text{ACDIF}(n) = \frac{(f \cdot g \oplus g)(n) + (f \oplus g \cdot g)(n) - 2(f \Theta g \circ g)(n)}{2}. \tag{10}$$

An enhanced morphology gradient operator (MGPO) [19]:

$$\begin{aligned}\text{MGPO}(n) &= G_{\text{C\&O}}(n) \cdot G_{\text{CO\&OC}}(n)\\ &= [(f \cdot g)(n) - (f \circ g)(n)]\\ &\quad \cdot [(f \cdot g \circ g)(n) - ((f \circ g \cdot g))(n)].\end{aligned} \tag{11}$$

2.2. Enhanced Combination Gradient Morphological Filter.

Dilation operator increases the valley of the signal and extends the peak, and erosion operator reduces the peak value of the signal and widens the valley. Opening operator suppresses peaks in the signal, removing glitches and isolated points on the upper edge of the signal. On the contrary, closing operator suppresses the valley in the signal, removing the glitch and isolated points of the lower edge of the signal. Therefore, according to the characteristics of the aforementioned operators, they are able to implement two functions for processing signals. One category can reduce negative impulse signals, and the other can reduce positive impulse signals [20].

Firstly, the cascades of dilation and closing are defined as follows:

$$\begin{aligned}F_{\text{DC}}(f(n)) &= (f \oplus g \cdot g)(n),\\ F_{\text{CD}}(f(n)) &= (f \cdot g \oplus g)(n).\end{aligned} \tag{12}$$

Secondly, the cascades of erosion and opening are defined as follows:

$$\begin{aligned}F_{\text{EO}}(f(n)) &= (f \Theta g \circ g)(n),\\ F_{\text{OE}}(f(n)) &= (f \circ g \Theta g)(n).\end{aligned} \tag{13}$$

F_{DC} and F_{CD} have been enhanced in suppressing the negative impulse and extracting the positive impulse of the signal. In contrast, F_{EO} and F_{OE} have been enhanced in suppressing the positive impulse and extracting the negative impulse of the signal. Therefore, the four new difference operators are defined as follows:

$$\begin{aligned}F_{\text{CD-OE}}(f(n)) &= (f \cdot g \oplus g)(n) - (f \circ g \Theta g)(n),\\ F_{\text{CD-EO}}(f(n)) &= (f \cdot g \oplus g)(n) - (f \Theta g \circ g)(n),\\ F_{\text{DC-OE}}(f(n)) &= (f \oplus g \cdot g)(n) - (f \circ g \Theta g)(n),\\ F_{\text{DC-EO}}(f(n)) &= (f \oplus g \cdot g)(n) - (f \Theta g \circ g)(n).\end{aligned} \tag{14}$$

The morphological operator introduced in Section 2.1, Lv et al. [20] combined the characteristics of four basic operators to propose an average combined difference operator (i.e., ACDIF), and he proved that the filtering effect of $F_{\text{CD-EO}}$ and $F_{\text{DC-EO}}$ is better than $F_{\text{CD-OE}}$ and $F_{\text{DC-OE}}$, which improves the extraction accuracy of fault signature signals. Li et al. [19] proposed the MGPO operator by summarizing the characteristics of operators; the MGPO operator further enhances the extraction capability of the morphological filtering fault signature by the product of two difference operators. Therefore,

to further enhance the ability to extract feature failures and extract fault characteristics under stronger background noise, this paper proposes a new enhanced combination gradient morphological operator (i.e., ECGMF) based on the characteristics of the two morphological operators:

$$\begin{aligned}\text{ECGMF}(n) &= F_{\text{CD-EO}}(n) \cdot F_{\text{DC-EO}}(n)\\ &= [(f \cdot g \oplus g)(n) - (f \Theta g \circ g)(n)] \cdot [(f \oplus g \cdot g)\\ &\quad \cdot (n) - (f \Theta g \circ g)(n)].\end{aligned} \tag{15}$$

A simulation signal $x_0 = \cos(60\pi t) + 1.5\cos(100\pi t)$ is used to illustrate the composition of ECGMF. The flowchart of the ECGMF algorithm is shown in Figure 1.

2.3. Multiscale Morphological Filter.

In order to make the analysis signal more accurate, multiscale analysis is applied. Let $g(m)$ be a unit SE and ε ($\varepsilon = 1, 2, \ldots, \lambda$) be the scale. The SE applied at this scale can be defined as

$$\varepsilon g(m) = \underbrace{g(m) \oplus g(m) \oplus \cdots \oplus g(m)}_{\lambda-1 \text{ times}}. \tag{16}$$

Multiscale dilation and erosion can be defined as

$$\begin{aligned}(f \oplus \varepsilon g)(n) &= \underbrace{f \oplus g \oplus g \oplus \cdots \oplus g(n)}_{\lambda-1 \text{ times}},\\ (f \Theta \varepsilon g)(n) &= \underbrace{f \Theta g \Theta g \Theta \cdots \Theta g(n)}_{\lambda-1 \text{ times}}.\end{aligned} \tag{17}$$

Then, the opening and closing operations of signal $f(n)$ with SE λg are further defined as follows:

$$\begin{aligned}(f \circ \lambda g)(n) &= ((f \Theta \lambda g) \oplus \lambda g)(n),\\ (f \cdot \lambda g)(n) &= ((f \oplus \lambda g) \Theta \lambda g)(n).\end{aligned} \tag{18}$$

Ultimately, the multiscale enhanced combination gradient morphological filter (MECGMF) at scale ε can be expressed as

$$\begin{aligned}\text{MECGMF}\big(f(n)_{\lambda g}\big) &= F_{\text{CD-EO}}\big(f(n)_{\lambda g}\big) \cdot F_{\text{DC-EO}}\big(f(n)_{\lambda g}\big)\\ &= [(f \cdot \lambda g \oplus \lambda g)(n) - (f \Theta \lambda g \circ \lambda g)(n)]\\ &\quad \cdot [(f \oplus \lambda g \cdot \lambda g)(n) - (f \Theta \lambda g \circ \lambda g)(n)].\end{aligned} \tag{19}$$

To further verify the ability of the proposed operator to extract fault frequencies at different scales, characteristic frequency intensity coefficient (CFIC) was introduced [25]:

$$C_{\text{CFI}} = \frac{\sum_{i=1}^{M} A_{if_C}}{\sum_{j=1}^{N} A_{f_j}}, \tag{20}$$

where A_{if_C} represents the amplitude of the ith fault frequency, A_{f_j} represents the amplitude of each j point, and M and N represent the numbers of fault frequency and total frequency spectrum, respectively. The CFIC is used to measure the performance of fault feature extraction. Here, the value of M is 5 and N is 200.

Analyze the vibration signal of Figure 2(d) in Section 4.1 using the enhance combination gradient morphological
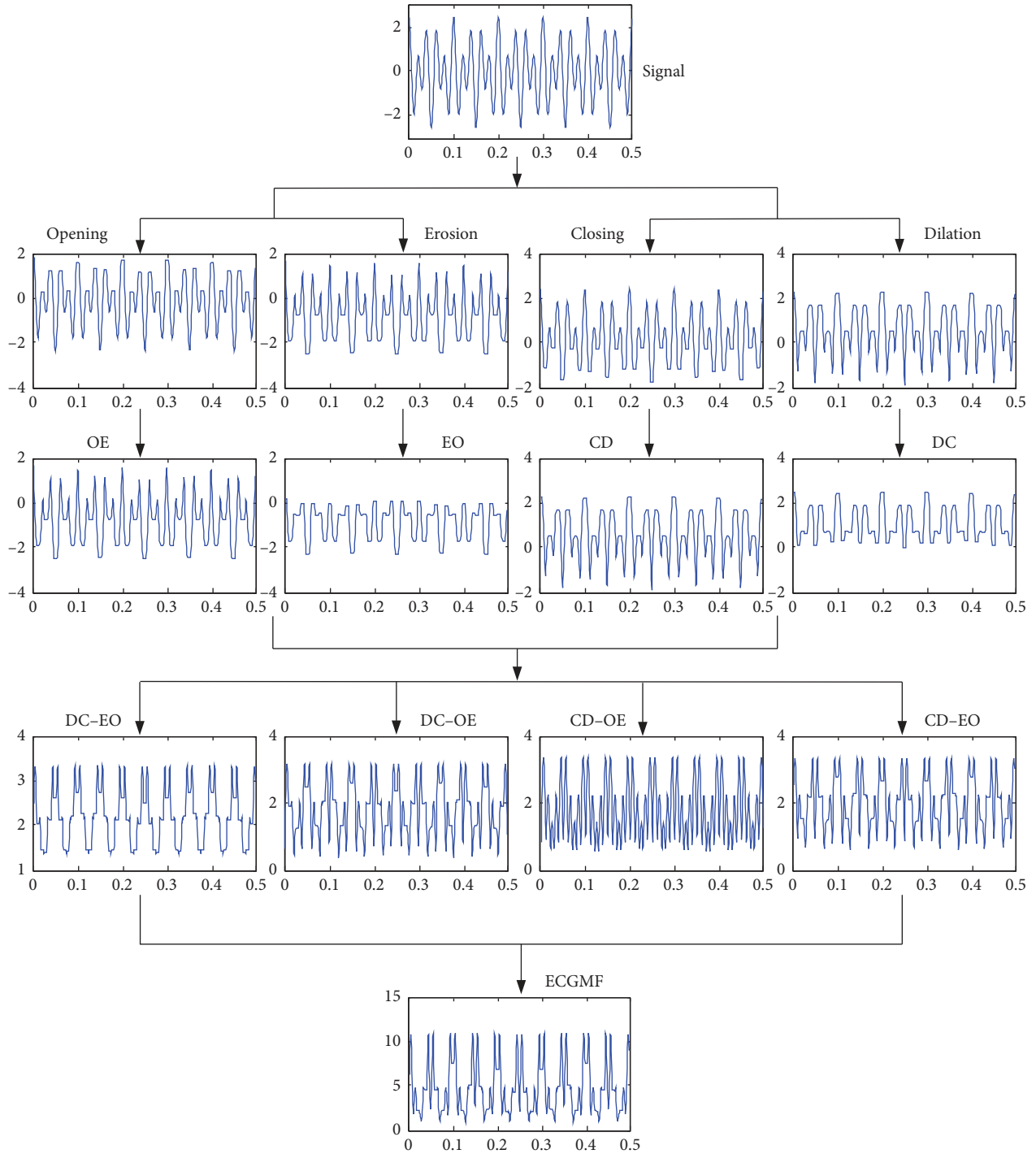
FIGURE 1: Process diagram of ECGMF calculation.

filter (ECGMF) and other proposed methods in Section 2.1. Figure 3 displays the CFIC of these methods. It can be found that the optimal CFIC value of $G_{CO\&OC}$ is 0.3124. Other four morphological filter operators (i.e., CMF, ACDIF, DIF, and MG) give better results than $G_{CO\&OC}$ analysis. The CFIC of the ECGMF varies with the scale. When the scale is 2, the maximum value is 0.4369.

When the scale is greater than 30, the performance of ECGMF is not as good as MG, but for the same set of fault signals, the smaller the scale, the more complete the fault information of the signal reservation. And, ECGMF gets the largest CFIC value at scale 2 compared to other operators. Therefore, the filtering performance of ECGMF is superior to other operators.

3. Proposed Adaptive Multiscale Enhanced Combination Gradient Morphology Filter

3.1. Adaptive Selection Strategy of SE Scale. A suitable SE scale plays a crucial role in the extraction of impulse signals
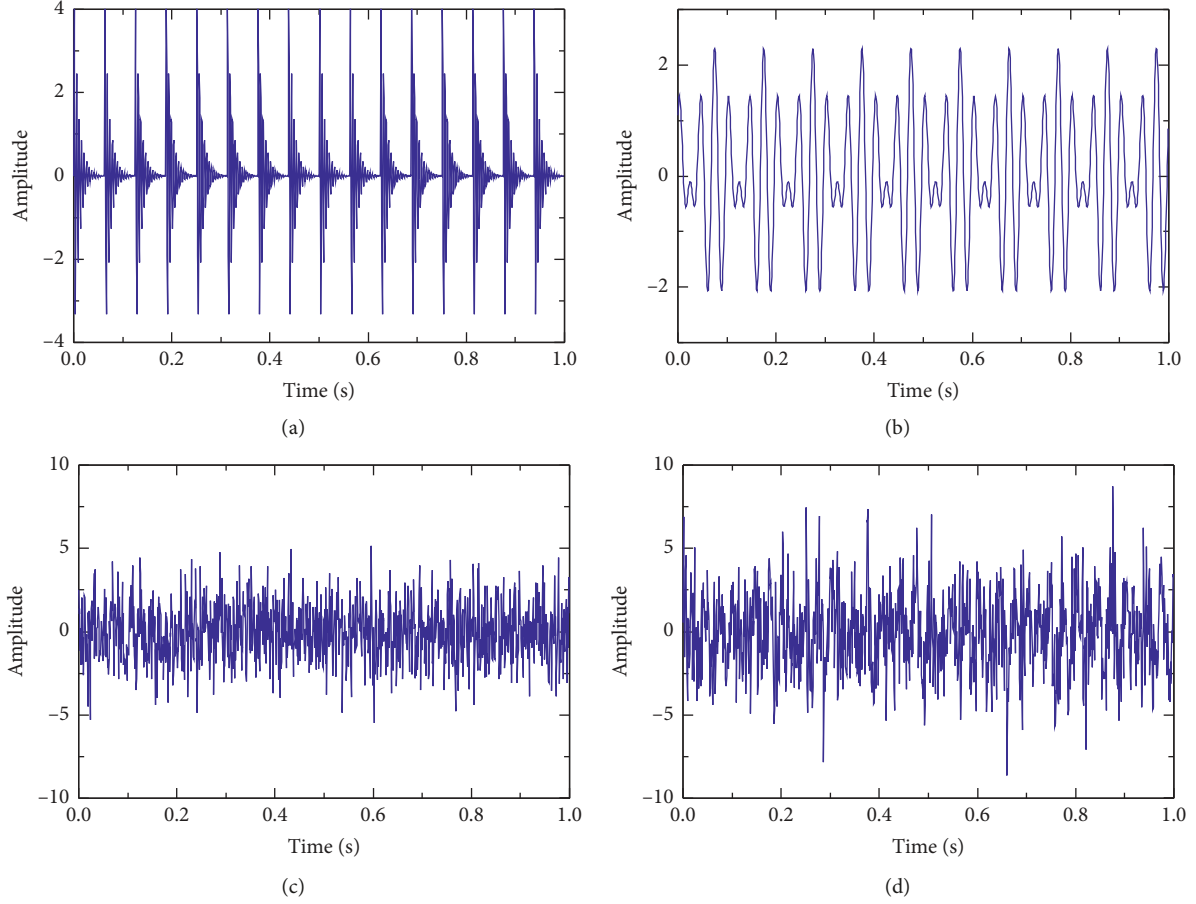
(a)

(b)

(c)

(d)

FIGURE 2: (a) Impulsive signal $y_2(t)$, (b) harmonic signal $y_1(t)$, (c) Gaussian white noise $\delta(t)$, and (d) simulation signal $y(t)$.

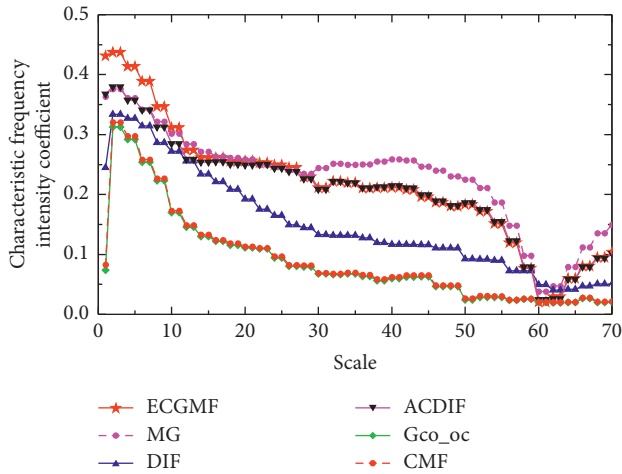FIGURE 3: Characteristic frequency intensity coefficients of ECGMF, MG, DIF, ACDIF, $G_{CO\text{-}OC}$, and CMF.

and the suppression of strong background noise. Most scholars [25, 26] used the average of the filtered results at each scale as the output:

$$y(n) = \frac{1}{\lambda} \sum_{\varepsilon=1}^{\lambda} y_\varepsilon(n). \tag{21}$$

In order to avoid all scales using the same weight results [27], this paper proposes an adaptive multiscale enhanced combination gradient morphological filter method (MECGMF):

$$\text{MECGMF}(y(n)) = \sum_{\lambda=1}^{\lambda_{max}} \left(\omega_\lambda \times \text{MECGMF}\left(f(n)_{\lambda g} \right) \right),$$

$$\omega_\lambda = \frac{e_\lambda}{\sum_{\lambda=1}^{\lambda_{max}} e_\lambda}, \quad e_\lambda = \sum_{n=0}^{N-1} \left| \text{MECGMF}\left(f(n)_{\lambda g} \right) \right|, \tag{22}$$

where ω_λ indicates the weight coefficient and e_λ represents the output of MECGMF at scale λ.

In addition to the MF operator, the choice of SE structure parameters is critical to the performance of the filter. In general, the shape and the height of SE have little effect on the filtering result. To improve the efficiency of calculation, this paper selected flat SE with zero height [27]. For a flat SE, as reported in [26], multiscale SEs are listed in Table 1.

The relationship between flat SE length and scale is $L = \lambda + 2$. The maximum selection length of SE should be f_s/f_o, where f_s represents sampling frequency and f_o represents fault frequency.

Kurtosis value is particularly sensitive to vibration shock signals and is particularly suitable for bearing surface damage diagnostics [28]. Its formula is as follows:

$$K = \frac{E(x-\mu)^4}{\sigma^4}, \qquad (23)$$

where x represents a discrete signal, μ represents an average value of x, and σ represents variance. Although kurtosis is an effective means of detection, it is also vulnerable to interferences. To solve this problem, Li et al. [23] proposed the frequency domain kurtosis. The formula is as follows:

$$K(y(f)) = \frac{1/n\sum_{i=1}^{n}\left(y_i(f)-\overline{y(f)}\right)^4}{\left(1/n\sum_{i=1}^{n}\left(y_i(f)-\overline{y(f)}\right)^2\right)^2}. \qquad (24)$$

In order to improve the performance of morphological filtering, Miao et al. [24] proposed another effective detection method named Hilbert envelope spectrum fault feature ratio R_f. It is defined as follows:

$$R_f = \frac{S(f)+S(2f)+S(3f)}{S}, \qquad (25)$$

where f represents the fault characteristic frequency and $S(f)$ represents the magnitude of the envelope spectrum at f.

Based on the advantages of the aforementioned two indicators, this paper proposes a new comprehensive measure called kurtosis fault feature ratio (KFFR). For a signal $y(f)$, KFFR is defined as follows:

$$KFFR = K_f \times R_f. \qquad (26)$$

KFFR is used for the detection of impulse signals, and it has strong anti-interference ability Therefore, KFFR is a comprehensive index which can be used to catch impulse features of the vibration signals. The larger the value of KFFR, the better filtering effect of the signal. Therefore, the largest KFFR is used to select the optimal SE scale of MECGMF.

3.2. Adaptive Multiscale Enhanced Combination Gradient Morphology Filter. This paper proposes a multiscale adaptive enhancement combination gradient morphological filtering method; the flowchart of this method for bearing fault diagnosis is depicted in Figure 4. The work steps are as follows:

Step 1: firstly, the vibration signal of the bearing under test is detected.

Step 2: then, calculating the scale range of MECGMF, the minimum scale is 1 and the maximum scale is $f_s/f_o - 2$.

Step 3: obtain the time-frequency domain analysis results of MECGMF under different SE scales.

Step 4: calculate the kurtosis value of the frequency domain and fault feature ratio (R_f) at each scale.

Step 5: calculate the kurtosis fault feature ratio (KFFR) results from step 4. The larger the value of KFFR is, the

TABLE 1: Multiscale structuring elements.

Scale	Double-dot structuring element	Flat structuring element
1	{1, 0, 1}	{0, 0, 0}
2	{1, 0, 0, 1}	{0, 0, 0, 0}
3	{1, 0, 0, 0, 1}	{0, 0, 0, 0, 0}
4	{1, 0, 0, 0, 0, 1}	{0, 0, 0, 0, 0, 0}
n	⋯	⋯

better the fault monitoring effect is and the stronger the noise suppression capability is.

Step 6: choose the optimal scale based on the maximum KFFR value and filtering the vibration signal from 1 to the optimal scale λmax.

Step 7: calculate the weighting coefficient of the signal at each scale based on step 6.

Step 8: obtain the final spectrum of the signal.

4. Simulation Study

4.1. Simulation Signal Analysis. To verify the effectiveness of the proposed method, a set of simulated signals is established. A periodic impulse vibration signal is generated when a local fault occurs in the rolling element bearing; however, these impulse signals are usually subject to interference; these interference components mainly include harmonic interference and white Gaussian noise. According to Xu et al. [29] and Zhang et al. [30], the failure model of the rolling bearing was established:

$$\begin{cases} y(t) = y_1(t) + y_2(t) + \delta(t), \\ y_1(t) = 1.2\sin(2f_1\pi t) + 1.1\cos(2f_2\pi t), \\ y_2(t) = 5\exp(-100t_1)\sin(400\pi t), t_1 = \mathrm{mod}\left(t, \frac{1}{f_o}\right), \end{cases} \qquad (27)$$

where harmonic frequency f_1 and f_2 are defined as 30 Hz and 40 Hz, respectively. The Gauss white noise signal $\delta(t)$ with -5 db SNR is added to the original signal. The fault frequency $f_o = 16$ Hz. The sampling frequency $f_s = 1024$ Hz, and the sampling number $N = 1024$.

The simulation signal $y(t)$, impulsive signal $y_2(t)$, harmonic signal $y_1(t)$, and Gaussian white noise $\delta(t)$ are shown in Figure 2. In Figure 2(d), the periodic impulse signal has been heavily flooded in the background noises. After analyzing $y(t)$, the FFT spectrum and envelope spectrum of $y(t)$ are shown in Figure 5. From Figure 5(a), interference frequencies f_1 and f_2 can be clearly seen. From Figure 5(b), due to the interference of background noise and harmonic signals, it is difficult to find the fault frequency f_o.

4.2. Analysis Result of MECGMF. The vibration signal of Figure 2(d) is processed by the method proposed in this paper. Firstly, the KFFR values at various scales are calculated, and the calculation results are shown in Figure 6. In
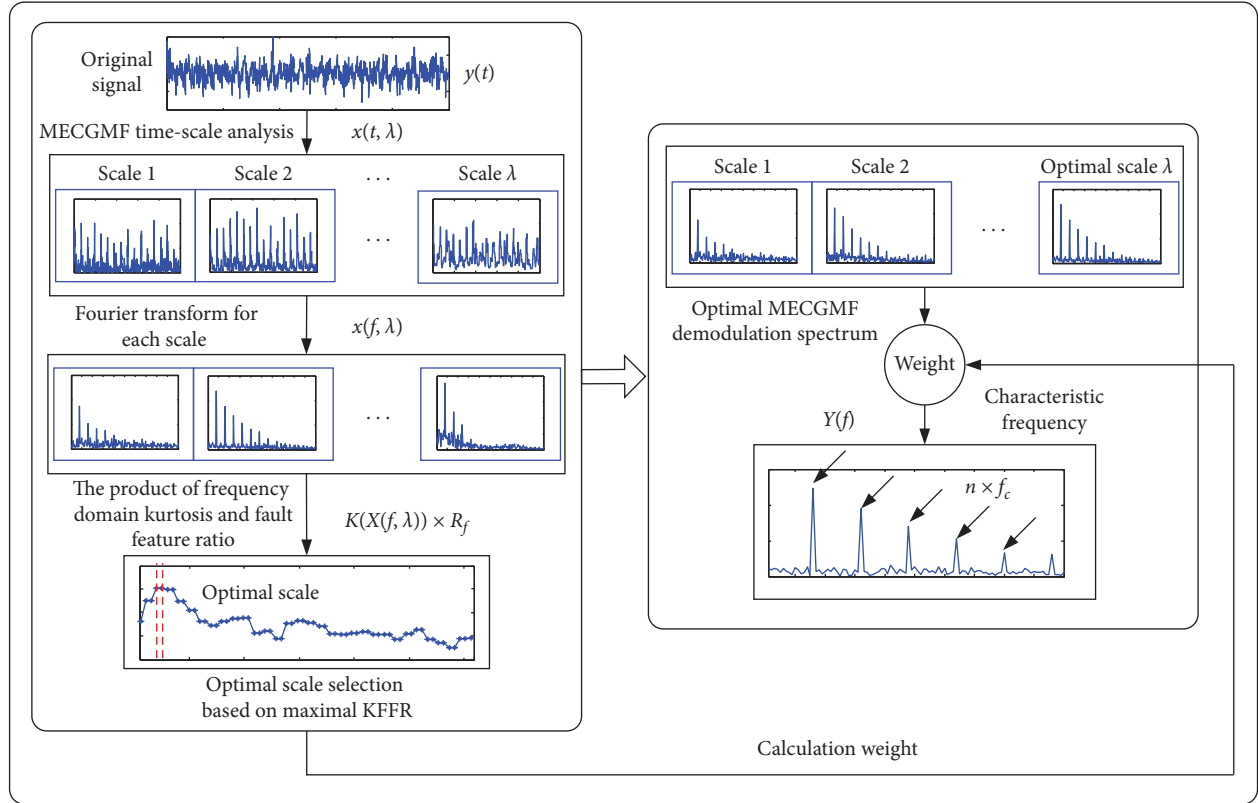
FIGURE 4: Flowchart of the proposed method for bearing defect detection.
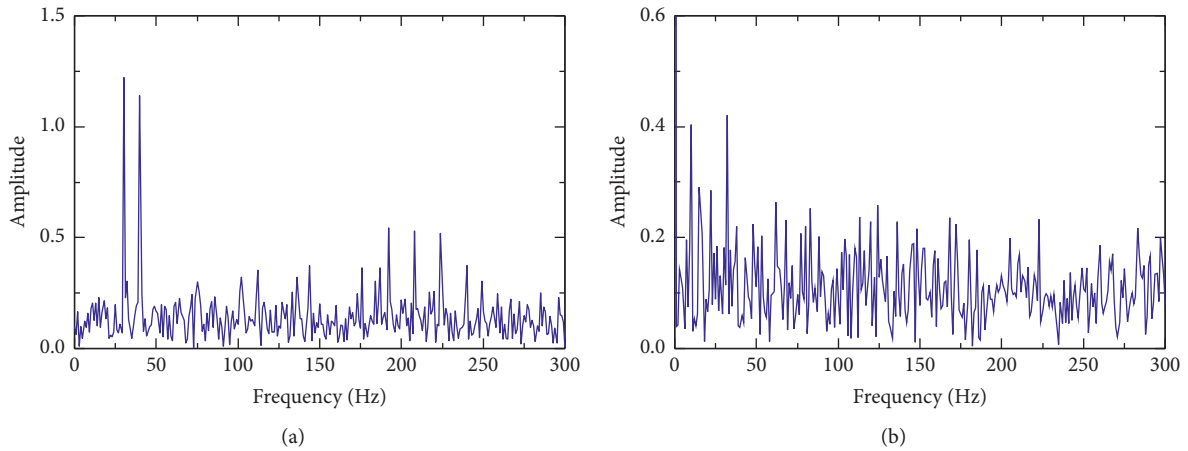

(a)

(b)

FIGURE 5: (a) FFT spectrum; (b) envelope spectrum for simulation signal $y(t)$.

Figure 6, when the scale $\lambda = 4$, KFFR takes the maximum value. Hence, the SE scale (i.e., $\lambda = 4$) is selected.

The results of the analysis of the signal $y(t)$ by the proposed method are shown in Figure 7. From Figure 7(b), the periodic impulsive characteristic frequencies (e.g., 16, 32, 48, 64, 80, and 96 Hz) are extracted and the interfering harmonic frequencies (30 and 40 Hz) are suppressed, the fault signature frequency can be clearly seen, and the background noise is effectively suppressed. The proposed method shows the accuracy of the extraction of bearing fault features.

For comparison verification, the same signal $y(t)$ is processed by the traditional multiscale morphology filter (MMF) [25, 26]. The average weight of the scale is expressed as 1/31. The analysis and processing results are shown in Figure 8. In Figure 8(b), fault frequencies 16 Hz and 32 Hz can be detected; other high-order fault frequencies (e.g., 64, 80, and 96 Hz) are not obvious. What is more, the suppression of noise interference is not good, and harmonic interference (e.g., 10 Hz = 40–30 Hz) still exists. Comparing Figure 7(b) and Figure 8(b), the proposed method is more effective in dealing with bearing fault frequencies.
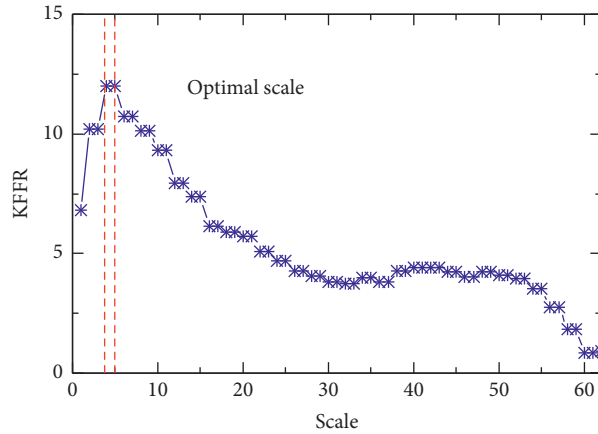
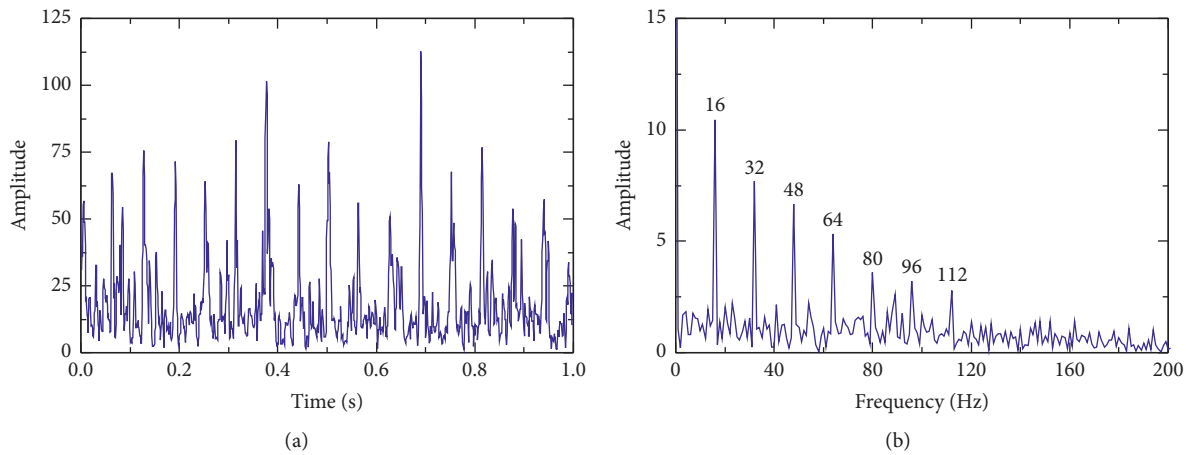FIGURE 6: KFFR values of filtering results with different scales.

(a)

(b)

FIGURE 7: Impulsive extracting results of the proposed MECGMF: (a) waveform; (b) frequency spectrum.

As mentioned earlier, Yan's method [27] is proved to be an effective fault detection method. Therefore, in order to further verify the accuracy of the method, it is compared with his method. In his method, flat SE is selected; the optimal scale of MCMFH is chosen by the feature energy factor (FEF) criterion; the relationship between SE scale and FEF is shown in Figure 9. From Figure 9, the maximum scale is 2.

The filtered result after processing is shown in Figure 10. In Figure 10(b), noise interference is large and high-order fault frequencies (e.g., 64, 80, and 96 Hz) are submerged in background noise. Comparing Figure 7(b) and Figure 10(b), the method proposed in this paper is more effective in fault feature extraction. Some quantitative indexes [11], for instance, kurtosis and energy ratio (ER) (i.e., the ratio of the fault frequency to the total spectrum) are calculated to evaluate the filtering ability of MECGMF.

Table 2 shows kurtosis and ERs (frequency band 0–200 Hz) of four methods on the simulation signal $y(t)$. After MECGMF processed, the kurtosis is 9.28 and the ER of the filtered signal is 51.37%. After MCMFH processed, the kurtosis is 3.65 and the ER of the filtered signal is 31.48%. After traditional MMF processed, the kurtosis is 2.56 and the

ER of the filtered signal is 25.11%. The kurtosis is 3.12 and the value of ER is 19.25% after envelope spectrum processed. The kurtosis after MCMFH processing is higher than the traditional MMF method and envelope spectrum analysis method. However, the MECGMF method proposed in this paper obtains the maximum kurtosis value of 9.28. At the same time, MECGMF obtains the largest ER value of 51.37%, which is 19.89% higher than the MCMFH method, 26.26% higher than the traditional MMF method, and 32.12% higher than the envelope spectrum method. It indicates that MECGMF extracts the signal fault characteristic frequency better and suppresses the noise interference greatly. From the aforementioned analysis results, MECGMF is superior to the other three methods in extracting the characteristic frequency and suppressing noise.

5. Experiment Validations

5.1. Case 1: Bearing with Inner Race Defect. In order to verify the validity of MECGMF, the bearing fault data from Case Western Reserve University (CWRU) [31] were firstly adopted. The experimental platform is shown in Figure 11; it consists of three parts: a 2-hp motor, a torque transducer,
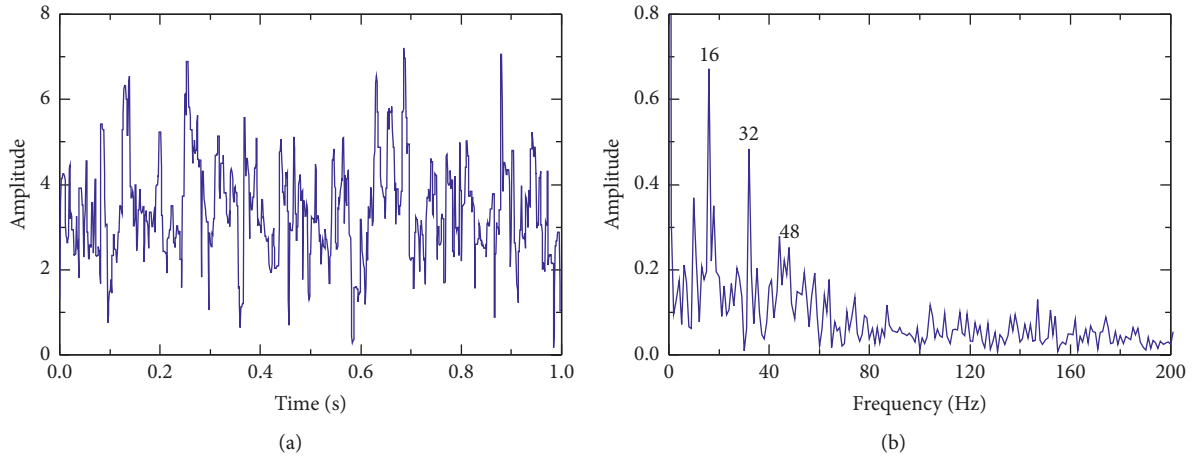
(a)

(b)

FIGURE 8: Impulsive extracting results of traditional MMF: (a) waveform; (b) frequency spectrum.
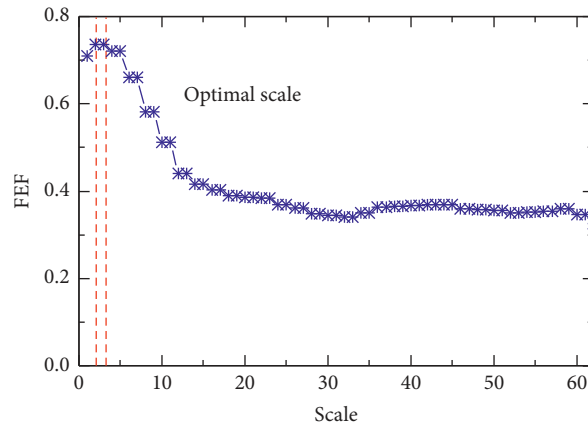

FIGURE 9: Relation curve between FEF and SE scale for simulation signal $y(t)$.
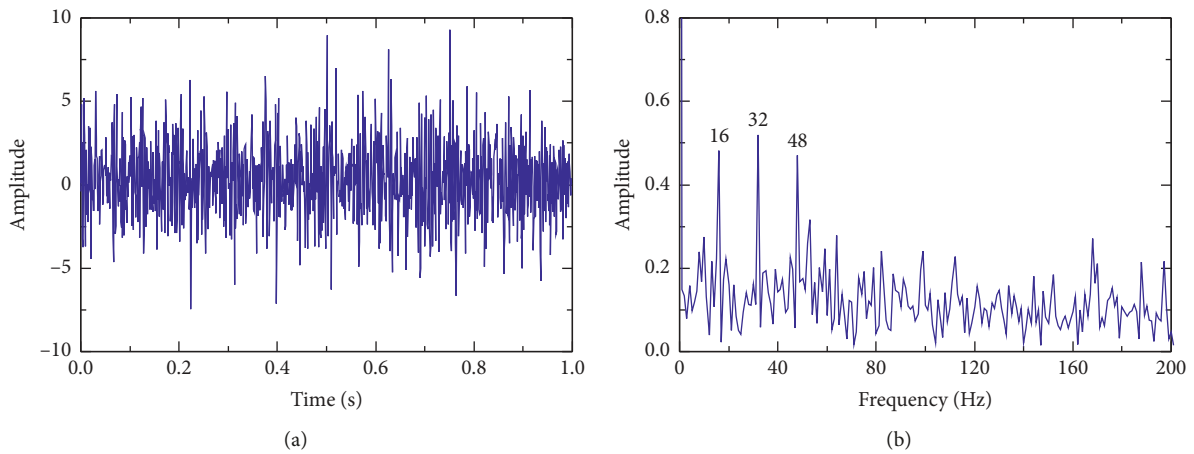

(a)

(b)

FIGURE 10: Impulsive extracting results of MCMFH: (a) waveform; (b) frequency spectrum.

and a dynamometer. The bearing model tested is 6205-2RS SKF and the speed of the motor is 1797 rpm; the structural parameters of the bearing are shown in Table 3. A 0.007 mm fault in diameter in the inner is generated using electro-discharge machining. The sampling frequency was 12000 Hz and sampling points are 2048, the theoretical calculation of the fault frequency (f_{BPFI}) of the inner race of the bearing is 162.4 Hz, and the rotational frequency (f_r) is 29.95 Hz. The formula for the theoretical calculation of the fault frequency (f_{BPFI}) of the inner race of the bearing is as follows:

Table 2: Comparison results of the MECGMF, MCMFH, traditional MMF, and envelope spectrum.

Methods	Kurtosis	ER (%)
MECGMF	9.28	51.37
MCMFH	3.65	31.48
Traditional MMF	2.56	25.11
Envelope spectrum	3.12	19.25

Figure 11: Bearing experimental platform.

$$f_{BPFI} = N \cdot f_r \cdot \frac{1 + D/d_m \cos \alpha}{2} = 162.4 \, \text{Hz}, \qquad (28)$$

where, N is the ball number, D is the ball diameter, d_m is the pitch diameter, and α is the contact angle.

The time-domain image of the experimental test signal and the processed frequency domain image are shown in Figure 12. In Figure 12(b), fault characteristic frequency is difficult to be found due to background noise interference. Therefore, it is important to extract the fault characteristic frequency of the bearing.

The vibration signal of Figure 12(a) is processed by the method proposed in this paper. Firstly, the KFFR values at various scales are calculated, and the calculation results are shown in Figure 13. In Figure 13, when the scale $\lambda = 6$, KFFR takes the maximum value. Hence, the SE scale (i.e., $\lambda = 6$) is selected. After applying the MECGMF method, the filtered signal and the frequency spectrum of the inner race fault are displayed in Figure 14.

The traditional MMF method is applied to process the experimental data of Figure 12(a). The average weight of the scale is expressed as 1/73. After applying the traditional MMF method, the time-domain signal and the frequency spectrum of the inner race fault are shown in Figure 15.

The MCMFH method is also applied to process the same vibration signal. And, the optimal scale of MCMFH is chosen to be 12. After applying the MCMFH method, the time-domain signal and the frequency spectrum of the inner race fault are displayed in Figure 16.

In Figure 14(b), we can clearly identify the fault characteristic frequency (i.e., 164.1 Hz) and the coupling frequency with the rotational frequency. In Figures 15(b) and 16(b), the fault characteristic frequency of the inner of the bearing is not obvious. The comparison results show that the ability of the MECGMF to extract the fault characteristics is stronger than the other two methods.

Table 4 shows kurtosis and ERs (frequency band 0–600 Hz) of four methods on the experimental signals. After

MECGMF processed, the kurtosis is 11.08 and the ER of the filtered signal is 41.63%. After MCMFH processed, the kurtosis is 6.75 and the ER of the filtered signal is 28.78%. After traditional MMF processed, the kurtosis is 2.79 and the ER of the filtered signal is 25.93%. The kurtosis is 5.51 and the value of ER is 21.61% after envelope spectrum processed. The MECGMF method proposed in this paper obtains the maximum kurtosis. At the same time, MECGMF obtains the largest ER value of 41.63%, which is 12.85% higher than the MCMFH method, 15.7% higher than the traditional MMF method, and 20.02% higher than the envelope spectrum method. From the above data comparison results can show that MECGMF extracts the signal fault characteristic frequency better and suppresses the noise interference greatly. From the aforementioned analysis results, MECGMF is superior to the other three methods in extracting the fault characteristic frequency and suppressing noise.

5.2. Case 2: Bearing with Outer Race Defect. In order to further verify the correctness and engineering applicability of the method proposed, wind turbines produced by the company are used to make a test. The wind turbine test bench is shown in Figure 17.

In Figure 17, the experimental system mainly includes wind power generator, data collector, electric control cabinet, acceleration sensor, and computer. Tested wind turbine is installed on the bench. The wind turbine model is a YJ93 A 1.5 MW doubly-fed asynchronous generator, and the rated speed is 1509 rpm. The data collector applied is RONDS, and the type of acceleration is B&K Vibro AS-020. The electric control cabinet provides power for the driving wind turbines, and the configuration of the computer is the same as the simulation. The acceleration sensor is mounted on the bearing end cap. The test bearing model is shown in Table 5. The sampling frequency is 16384 Hz; the theoretical calculation of the fault frequency (f_{BPFO}) of the outer race of the bearing is 53.2 Hz.

The vibration signal of the bearing outer ring and its spectrum diagram are shown in Figures 18(a) and 18(b), respectively. In Figure 18(b), it is difficult to find the fault characteristic frequency of the bearing outer ring.

The method proposed in this paper (MECGMF) is applied to process the data in Figure 18(a). At first, the KFFR values at various scales are calculated, and the calculation results are shown in Figure 19. From Figure 19, the optimal scale is 68. Then, the analysis result and the corresponding spectrum are shown in Figure 20. From Figure 20(a), we can see the periodic shock signal, and the impact characteristics of the signal are enhanced; the filtering effect is obvious. In Figure 20(b), wind turbines are subject to low-frequency interference during operation, and fault features are easily submerged in background noise. In the range of 0–100 Hz, the frequency components are more complicated. Since the MECGMF method uses the product of two differential morphological operators, it has an enhanced effect on fault feature extraction, so it is sensitive to the fault impact signal, and the fault frequency f_{BPFO} of the bearing outer ring can be clearly detected. In addition to 100 Hz, the MECGMF

TABLE 3: Structural parameters of the bearing.

Outer diameter (mm)	Inside diameter (mm)	Thickness (mm)	Pitch diameter (mm)	Ball diameter (mm)	Ball number	Contact angle (°)
52	25	15	39	8	9	0

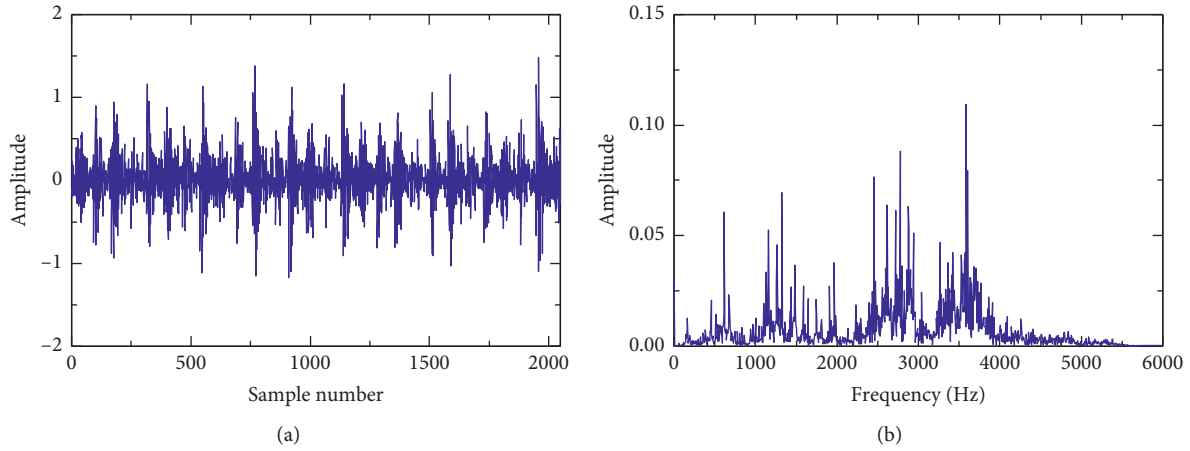(a)   (b)

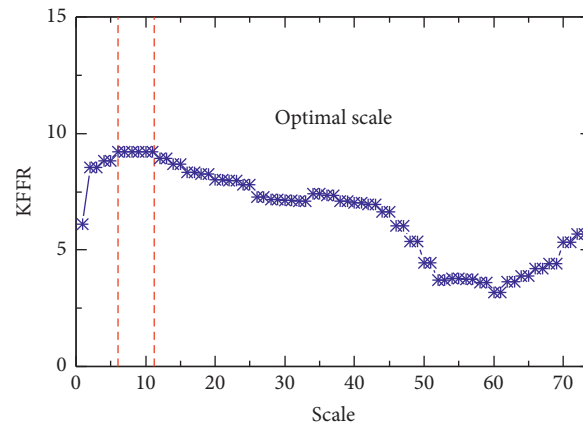FIGURE 12: Waveform and amplitude spectrum of the inner race defect signal: (a) time-domain waveform; (b) amplitude spectrum.

FIGURE 13: Case 1: KFFR values of filtering results with different scales.

(a)   (b)
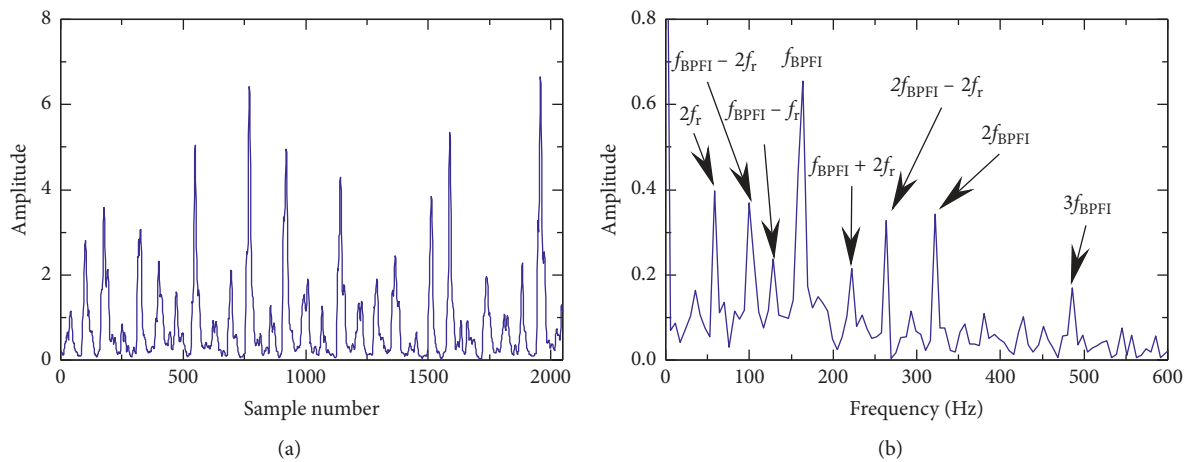
FIGURE 14: Case 1: waveform and spectrum of the MECGMF filtering result: (a) time-domain waveform; (b) amplitude spectrum.
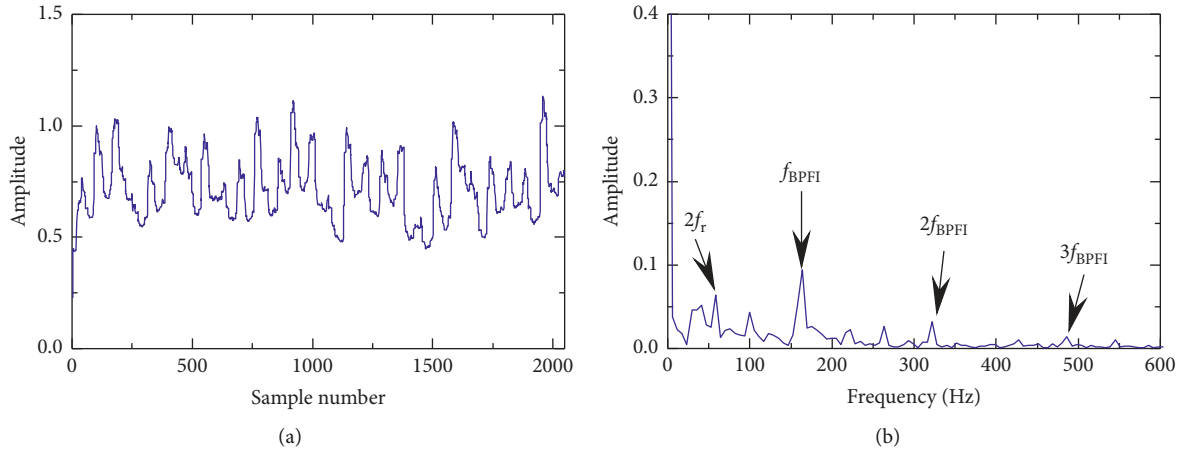
FIGURE 15: Case 1: waveform and spectrum of the traditional MMF filtering result: (a) time-domain waveform; (b) amplitude spectrum.
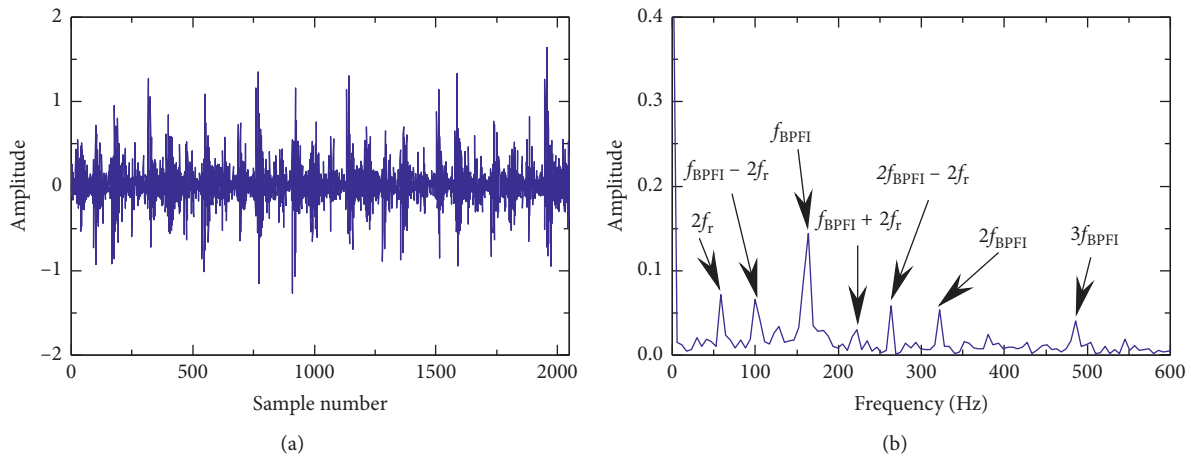
FIGURE 16: Case 1: waveform and spectrum of the MCMFH filtering result: (a) time-domain waveform; (b) amplitude spectrum.

TABLE 4: Case 1: comparison results of the MECGMF, MCMFH, traditional MMF, and envelope spectrum.

Methods	Kurtosis	ER (%)
MECGMF	11.08	41.63
MCMFH	6.75	28.78
Traditional MMF	2.79	25.93
Envelope spectrum	5.51	21.61

method has superior filtering performance, and harmonic frequencies ($2f_{BPFO}$, $3f_{BPFO}$, $4f_{BPFO}$, and $5f_{BPFO}$) can be clearly detected. Therefore, the method proposed in this paper can effectively detect the fault characteristics of wind turbine bearings.

The traditional MMF method is applied to process the experimental data of Figure 18(a). The weight of each scale is 1/120. Filter processing result of inner race is displayed in Figure 21. From Figure 21(b), the fault frequency f_{BPFO} of the bearing and its harmonic frequency $3f_{BPFO}$ can be detected, and other harmonic frequencies are submerged in the noise interference.

The same experimental signal was processed by method MCMFH. According to the FEF criterion, the optimal SE scale of the MCMFH method is 110. After analyzing, filter processing result of the outer ring of the bearing is shown in Figure 22. In Figure 22(b), the fault signal of the bearing is almost drowned in the background noise.

Comparing Figure 20(b) with Figures 21(b) and 22(b), we can clearly see that the method proposed in this paper (MECGMF) is more effective than the other two methods in dealing with bearing failures. The traditional MMF method and the MCMFH method have no obvious effect on strong background noise filtering. A large number of
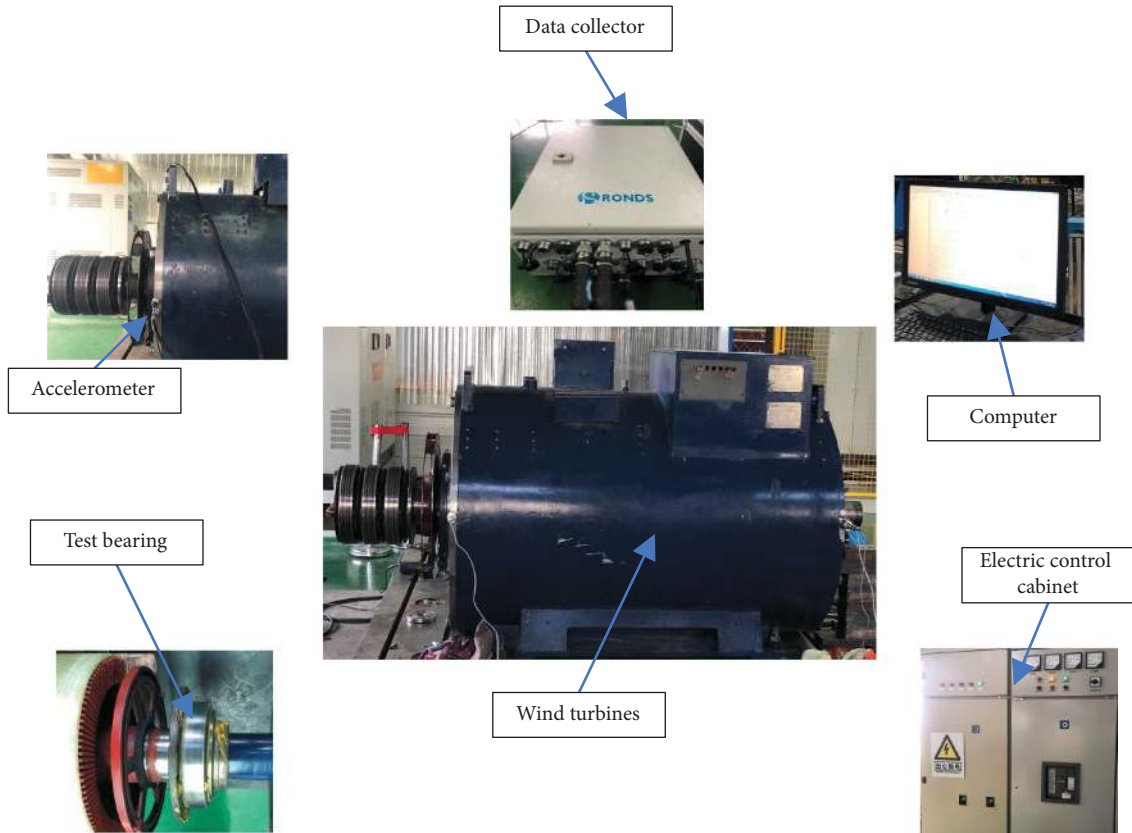
FIGURE 17: Wind turbine experimental platform.

TABLE 5: Structural parameters of the bearing.

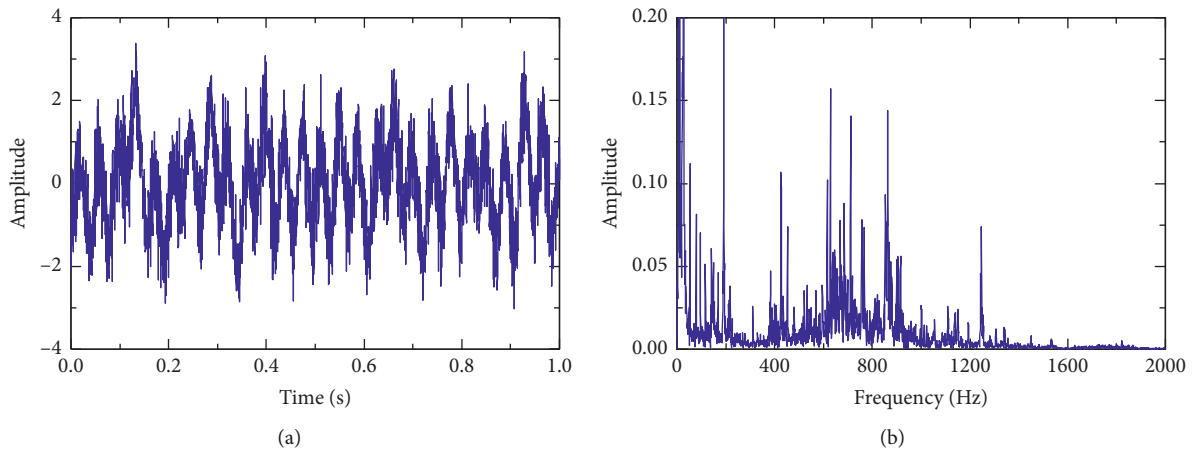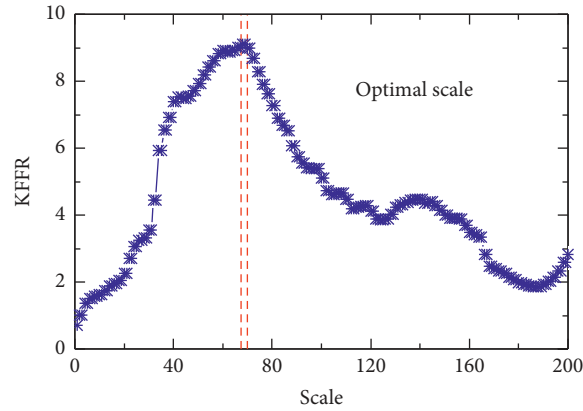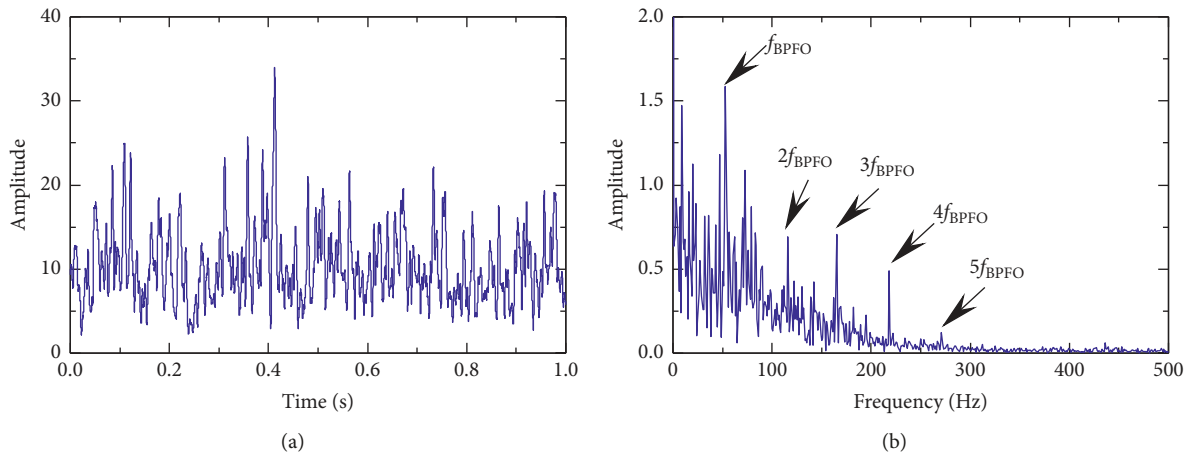| Outer diameter (mm)	Inside diameter (mm)	Thickness (mm)	Pitch diameter (mm)	Ball diameter (mm)	Ball number	Contact angle (°)
340	160	68	250	50.8	9	0

(a)

(b)

FIGURE 18: Waveform and amplitude spectrum of the outer race defect signal: (a) time-domain waveform; (b) amplitude spectrum.

Figure 19: Case 2: KFFR values of filtering results with different scales.

(a)

(b)

Figure 20: Case 2: waveform and spectrum of MECGMF filtering result: (a) time-domain waveform; (b) amplitude spectrum.
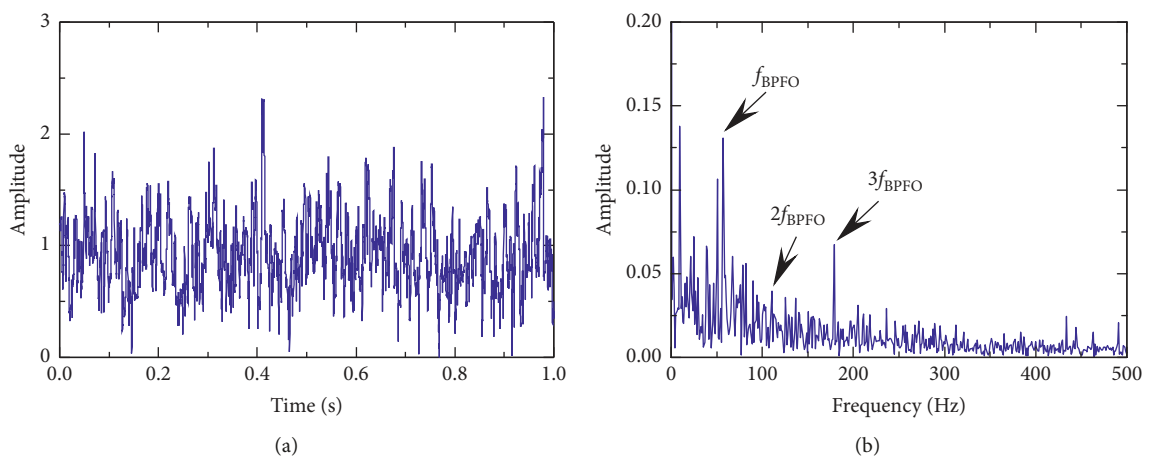

(a)

(b)

Figure 21: Case 2: waveform and spectrum of traditional MMF filtering result: (a) time-domain waveform; (b) amplitude spectrum.

frequency interference components can be detected in the frequency range of 100–500 Hz. This causes the harmonic frequencies ($2f_{BPFO}$, $3f_{BPFO}$, $4f_{BPFO}$, and $5f_{BPFO}$) of the fault frequency to be contaminated and submerged in the

background noise. Wind turbine bearing faults are often subject to severe low-frequency noise disturbances. Therefore, MECGMF is effective in engineering applicability.
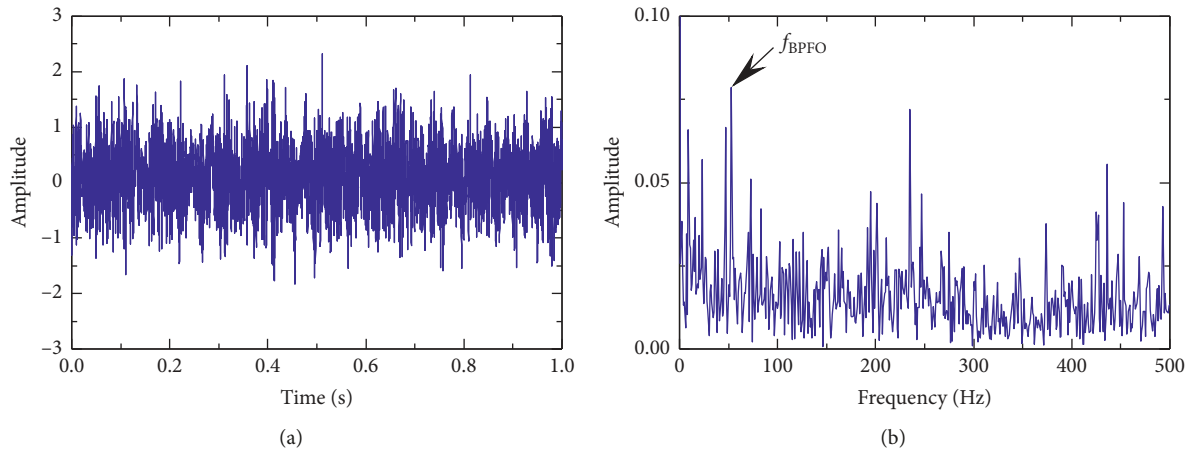
FIGURE 22: Case 2: waveform and spectrum of MCMFH filtering result: (a) time-domain waveform; (b) amplitude spectrum.

6. Conclusions

In this paper, a new adaptive multiscale enhanced combination gradient morphological filter (MECGMF) is proposed for rolling element bearing fault diagnosis. An enhanced combination gradient morphological operation (ECGMF) is first built according to the ability of extracting fault characteristic information based on the two optimal combination difference operators. This method enhances noise rejection and the ability to extract fault information from the background noise of a stronger degree. A new comprehensive dimensionless index (KFFR) is proposed to select the optimal scale of MECGMF, which further strengthens the self-adaptive ability. The simulation and experimental results show that the MECGMF is effective for bearing fault diagnosis. Comparative experiments show that MECGMF gives better detection ability, more effective in solving engineering issues.

Data Availability

The vibration time-domain signal data of the inner ring of the bearing come from Case Western Reserve University, and the fault data of the bearing outer ring used to support the findings of this study are available from the corresponding author upon request.

Conflicts of Interest

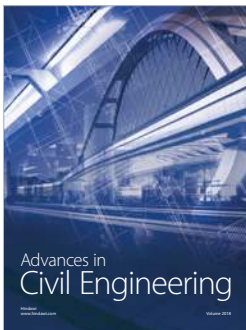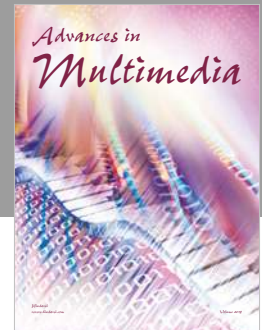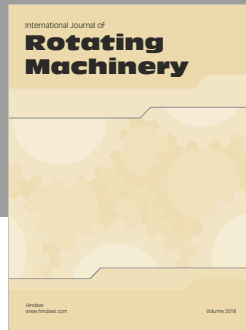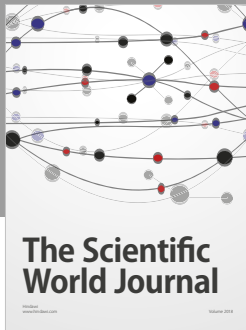The authors declare that they have no conflicts of interest.

Acknowledgments

References

[1] J. Zheng, "Rolling bearing fault diagnosis based on partially ensemble empirical mode decomposition and variable predictive model-based class discrimination," *Archives of Civil and Mechanical Engineering*, vol. 16, no. 4, pp. 784–794, 2016.

[2] S. Zhang, Y. Wang, S. He, and Z. Jiang, "Bearing fault diagnosis based on variational mode decomposition and total variation denoising," *Measurement Science and Technology*, vol. 27, no. 7, Article ID 075101, 2016.

[3] R. K. Vashisht and Q. Peng, "Crack detection in the rotor ball bearing system using switching control strategy and short time fourier transform," *Journal of Sound and Vibration*, vol. 432, pp. 502–529, 2018.

[4] P. Xia, H. Xu, M. Lei, and Z. Ma, "An improved stochastic resonance method with arbitrary stable-state matching in underdamped nonlinear systems with a periodic potential for incipient bearing fault diagnosis," *Measurement Science and Technology*, vol. 29, no. 8, Article ID 085002, 2018.

[5] J. Chen, J. Pan, Z. Li, Y. Zi, and X. Chen, "Generator bearing fault diagnosis for wind turbine via empirical wavelet transform using measured vibration signals," *Renewable Energy*, vol. 89, pp. 80–92, 2016.

[6] J. Dybała and R. Zimroz, "Rolling bearing diagnosing method based on empirical mode decomposition of machine vibration signal," *Applied Acoustics*, vol. 77, pp. 195–203, 2014.

[7] J. Serra, "Morphological filtering: an overview," *Signal Processing*, vol. 38, no. 1, pp. 3–11, 1994.

[8] J. Serra, "Image analysis and mathematical morphology," *Academic Emergency Medicine*, vol. 4, no. 2, pp. 184-185, 1983.

[9] S. Dong, L. Chen, B. Tang, X. Xu, Z. Gao, and J. Liu, "Rotating machine fault diagnosis based on optimal morphological filter and local tangent space alignment," *Shock and Vibration*, vol. 2015, Article ID 893504, 9 pages, 2015.

[10] C. Li and M. Liang, "Continuous-scale mathematical morphology-based optimal scale band demodulation of impulsive feature for bearing defect diagnosis," *Journal of Sound and Vibration*, vol. 331, no. 26, pp. 5864–5879, 2012.

[11] Y. Li, X. Liang, and M. J. Zuo, "A new strategy of using a time-varying structure element for mathematical morphological filtering," *Measurement*, vol. 106, pp. 53–65, 2017.

[12] Z. Chen, N. Gao, W. Sun et al., "A signal based triangular structuring element for mathematical morphological analysis and its application in rolling element bearing fault diagnosis," *Shock and Vibration*, vol. 2014, Article ID 590875, 16 pages, 2014.

[13] Z. Hu, C. Wang, J. Zhu, X. Liu, and F. Kong, "Bearing fault diagnosis based on an improved morphological filter," *Measurement*, vol. 80, pp. 163–178, 2016.

[14] B. Li, P.-L. Zhang, Z.-J. Wang, S.-S. Mi, and D.-S. Liu, "A weighted multi-scale morphological gradient filter for rolling

element bearing fault detection," *ISA Transactions*, vol. 50, no. 4, pp. 599–608, 2011.

[15] A. S. Raj and N. Murali, "Early classification of bearing faults using morphological operators and fuzzy inference," *IEEE Transactions on Industrial Electronics*, vol. 60, no. 2, pp. 567–574, 2013.

[16] S. Osman and W. Wang, "A morphological Hilbert-Huang transform technique for bearing fault detection," *IEEE Transactions on Instrumentation and Measurement*, vol. 65, no. 11, pp. 2646–2656, 2016.

[17] J. Wang, G. Xu, Q. Zhang, and L. Liang, "Application of improved morphological filter to the extraction of impulsive attenuation signals," *Mechanical Systems and Signal Processing*, vol. 23, no. 1, pp. 236–245, 2009.

[18] H. Aijun, L. Jianfeng, S. Shangfei, and X. Ling, "A novel approach of impulsive signal extraction for early fault detection of rolling element bearing," *Shock and Vibration*, vol. 2017, Article ID 9375491, 11 pages, 2017.

[19] Y. Li, M. J. Zuo, Y. Chen, and K. Feng, "An enhanced morphology gradient product filter for bearing fault detection," *Mechanical Systems and Signal Processing*, vol. 109, pp. 166–184, 2018.

[20] J. Lv and J. Yu, "Average combination difference morphological filters for fault feature extraction of bearing," *Mechanical Systems and Signal Processing*, vol. 100, pp. 827–845, 2018.

[21] F. Deng, S. Yang, G. Tang, R. Hao, and M. Zhang, "Self adaptive multi-scale morphology AVG-hat filter and its application to fault feature extraction for wheel bearing," *Measurement Science and Technology*, vol. 28, no. 4, Article ID 045011, 2017.

[22] X. Wu, M. Yang, and E. Al, "Bearing fault diagnosis using EEMD and improved morphological filtering method based on kurtosis criterion," *Journal of Vibration and Shock*, vol. 34, no. 2, pp. 38–44, 2015.

[23] Y. Li, M. J. Zuo, J. Lin, and J. Liu, "Fault detection method for railway wheel flat using an adaptive multiscale morphological filter," *Mechanical Systems and Signal Processing*, vol. 84, pp. 642–658, 2017.

[24] Y. Miao, M. Zhao, J. Lin, and Y. Lei, "Application of an improved maximum correlated kurtosis deconvolution method for fault diagnosis of rolling element bearings," *Mechanical Systems and Signal Processing*, vol. 92, pp. 173–195, 2017.

[25] B. Li, P.-L. Zhang, Z.-J. Wang, S.-S. Mi, and Y.-T. Zhang, "Gear fault detection using multi-scale morphological filters," *Measurement*, vol. 44, no. 10, pp. 2078–2089, 2011.

[26] Q. Chen, Z. Chen, W. Sun, G. Yang, A. Palazoglu, and Z. Ren, "A new structuring element for multi-scale morphology analysis and its application in rolling element bearing fault diagnosis," *Journal of Vibration and Control*, vol. 21, no. 4, pp. 765–789, 2013.

[27] X. Yan, M. Jia, W. Zhang, and L. Zhu, "Fault diagnosis of rolling element bearing using a new optimal scale morphology analysis method," *ISA Transactions*, vol. 73, pp. 165–180, 2018.

[28] D. Goyal, B. S. Vanraj, and S. S. Dhami, "Condition monitoring parameters for fault diagnosis of fixed axis gearbox: a review," *Archives of Computational Methods in Engineering*, vol. 24, no. 3, pp. 543–556, 2016.

[29] Y. Xu, K. Zhang, C. Ma, X. Li, and J. Zhang, "An improved empirical wavelet transform and its applications in rolling bearing fault diagnosis," *Applied Sciences*, vol. 8, no. 12, p. 2352, 2018.

[30] L. Zhang, J. Xu, J. Yang, and D. Yang, "Multiscale morphology analysis and its application to fault diagnosis," *Mechanical Systems and Signal Processing*, vol. 22, no. 3, pp. 597–610, 2008.

[31] Case Western Reserve University Bearing Data Center Website [EB/OL], 2011, http://csegroups.case.edu/bearingdatacenter/pages/download-data-file.